Available online at www.sciencedirect.com
SCIENCE DIRECT
ELSEVIER International Communications in Heat and Mass Transfer 32 (2005) 1211–1220
International Communications in HEAT and MASS TRANSFER
www.elsevier.com/locate/ichmt

Fully developed laminar flow and heat transfer in smooth trapezoidal microchannel☆

Bin Cao, Guang Wen Chen*, Quan Yuan

Dalian Institute of Chemical Physics, Chinese Academy of Sciences, 457 Zhongshan Road, Dalian 116023, China

Available online 6 June 2005

Abstract

Numerical analysis of fully developed laminar slip flow and heat transfer in trapezoidal micro-channels has been studied with uniform wall heat flux boundary conditions. Through coordinate transformation, the governing equations are transformed from physical plane to computational domain, and the resulting equations are solved by a finite-difference scheme. The influences of velocity slip and temperature jump on friction coefficient and Nusselt number are investigated in detail. The calculation also shows that the aspect ratio and base angle have significant effect on flow and heat transfer in trapezoidal micro-channel.

Keywords: Trapezoidal; Micro-channels; Slip flow

1. Introduction

In the past two decades, the rapid development of microelectromechanic systems (MEMS) and micro-chemical system has brought up a great interest in studying flow and heat transfer in micro-scale [1]. The Knudsen number Kn can classify the gas flow in micro-channel into four flow regimes: continuum flow regime ($Kn<0.001$), slip flow regime ($0.001<Kn<0.1$), transition flow regime ($0.1<Kn<10$) and free molecular flow regime ($Kn>10$).

In order to understand the characteristics of fluid flow and heat transfer in microchannel, many researchers have conducted experimental investigations in recent years. Wu and Little [2] measured the

☆ Communicated by P. Cheng and W.Q. Tao.

* Corresponding author.
E-mail address: gwchen@dicp.ac.cn (G.W. Chen).

0735-1933/$ - see front matter © 2005 Elsevier Ltd. All rights reserved.
doi:10.1016/j.icheatmasstransfer.2005.05.008

friction factors of nitrogen, argon and helium flow in trapezoidal microchannels. The depth range from 130 to 200 μm and the width was 30–60 μm. They found these friction factors were much larger than the predictions by the classic theory for laminar flow in conventional channels. Pfahler et al. [3,4] found that for microchannels with hydraulic diameters of 0.98–39.7 μm, and that the friction factors were lower than those predicted by the classic theory. Choi et al. [5] investigated the flow resistance of nitrogen gas flow in microtubes with hydraulic diameters between 3 and 81 μm, and found that the measured friction factors were smaller than those predicted by the classic theory.

Previous works [6] indicated that transport phenomena in the slip flow regime can be modeled by Navier-Stokes equations with boundary conditions that take into account the velocity slip and temperature jump at the wall. Theoretical and experimental analysis on slip flow in circular and rectangular microchannels has already been studied by many researchers [7,8]. However, slip flow in trapezoidal microchannels has not yet been investigated, in spite of its wide application in many Si-base MEMS [9].

The motivation of this paper is to study the fully developed laminar flow and heat transfer characteristics in the slip flow regime of trapezoidal microchannels. Through coordinate transformation, the governing equations on the computational domain are solved with uniform heat flux boundary conditions by a finite-difference scheme. The influences of velocity slip, temperature jump, and aspect ratio and base angle on friction coefficient and Nusselt number are investigated in detail.

2. Analysis

2.1. Problem statement and governing equations

We consider a Newtonian flow and heat transfer at slip flow regime in a trapezoidal microchannel. For the fully developed laminar steady state flow, ignoring body forces and viscous dissipation, the steady-state governing equations of momentum and energy can be written as

$$\frac{\partial^2 u}{\partial \tilde{x}^2}+\frac{\partial^2 u}{\partial \tilde{y}^2}=\frac{D_h^2}{L\mu}\frac{\partial P}{\partial \tilde{z}} \tag{1}$$

$$\frac{\partial \Theta}{\partial \tilde{z}}=\frac{1}{RePr\varepsilon}\frac{\bar{u}}{u(\tilde{x},\tilde{y})}\left(\frac{\partial^2 \Theta}{\partial \tilde{x}^2}+\frac{\partial^2 \Theta}{\partial \tilde{y}^2}\right). \tag{2}$$

Where Re, Pr is the Reynolds number and the Prandtl number, respectively, and the dimensionless variables are defined as

$$\tilde{x}=x/D_h,\tilde{y}=y/D_h,\tilde{z}=z/L,\varepsilon=D_h/L. \tag{3}$$

For the case of uniform wall heat flux, the dimensionless temperature is defined as

$$\Theta=\frac{T-T_{in}}{qD_h/k},\Theta_{in}=0,\left.\frac{\partial \Theta}{\partial \tilde{n}}\right|_{wall}=-1 \tag{4}$$

2.2. Slip-flow boundary conditions at the wall

The slip velocity and temperature jump boundary conditions to the first order are expressed as

$$u|_{\text{wall}} = -\beta_v Kn \frac{\partial u}{\partial \tilde{n}}\Big|_{\text{wall}}, \Theta\Big|_{\text{wall}} - \Theta_{\text{wall}} = -\beta_T Kn \frac{\partial \Theta}{\partial \tilde{n}}\Big|_{\text{wall}} \tag{5}$$

Where

$$\beta_v = \frac{2-\sigma_v}{\sigma_v}, \beta_T = \frac{2-\sigma_T}{\sigma_T}\frac{2\gamma}{\gamma+1}\frac{1}{Pr}, \beta = \frac{\beta_T}{\beta_v} \tag{6}$$

In these equations, σ_v is the tangential momentum accommodation coefficient, and is considered to vary between 0 and 1, and σ_T is the thermal accommodation coefficient, which typically has a range from 0.01 to 1.The parameters, β_v and β_T indicate the influence of rarefaction and fluid-surface interaction. For typical engineering application, the value of the ratio β is close to 1.667 [7,8]. In the following of this paper we use parameter β instead of parameter β_T.

2.3. Coordinate transformation

In order to convert the trapezoidal cross-section into a square cross-section, we transfer the independent variables on physical plane (x, y) to a new set of independent variables in computational plane (ξ, η) as shown in Fig. 1 where

$$\xi = \frac{(a+x)H + (b-a)y}{2((b-a)y + aH)} \tag{7}$$

$$\eta = y/H \tag{8}$$

With the above coordinative system transformation, governing equations on computational domain can be expressed as

$$\frac{\partial^2 \phi}{\partial \tilde{x}^2} + \frac{\partial^2 \phi}{\partial \tilde{y}^2} = C_1 \frac{\partial^2 \phi}{\partial \xi^2} + C_2 \frac{\partial^2 \phi}{\partial \eta^2} + C_3 \frac{\partial^2 \phi}{\partial \xi \partial \eta} + C_4 \frac{\partial \phi}{\partial \xi} + C_5 \frac{\partial \phi}{\partial \eta} \tag{9}$$

C_1, C_2, C_3, C_4, C_5 are the coefficients in the transformed governing equation, and are obtained from

$$C_1 = \alpha_1/J^2, C_2 = \gamma_1/J^2, C_3 = -2\beta_1/J^2, C_4 = \xi_y'', C_5 = 0 \tag{10}$$

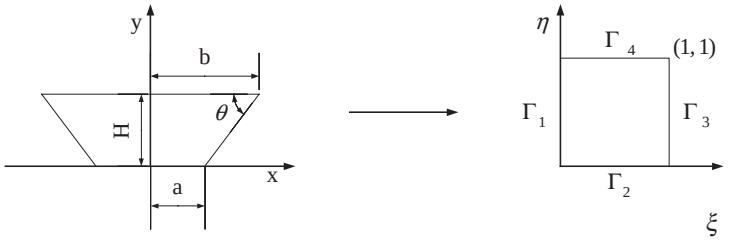

Fig. 1. Transformation of a trapezoid on physical plane to a square on the computational plane.

Where α_1, β_1, γ_1 and J are given by

$$\alpha_1 = x_\eta^2 + y_\eta^2, \beta_1 = x_\xi x_\eta + y_\xi y_\eta, \gamma_1 = x_\xi^2 + y_\xi^2, J = x_\xi y_\eta - y_\xi x_\eta. \tag{11}$$

The local normal gradient at the wall on computational domain is expressed as [10]

$$\frac{\partial \phi}{\partial \tilde{n}^{(\eta)}} = \frac{\gamma_1 \phi_\eta - \beta_1 \phi_\xi}{J\sqrt{\gamma_1}}, \frac{\partial \phi}{\partial \tilde{n}^{(\xi)}} = \frac{\alpha_1 \phi_\xi - \beta_1 \phi_\eta}{J\sqrt{\alpha_1}}. \tag{12}$$

2.4. Calculation of friction coefficient and Nusselt number

The main flow mean velocity and temperature in the cross-section are

$$\bar{u} = \frac{\int\int u J \mathrm{d}\xi \mathrm{d}\eta}{\int\int J \mathrm{d}\xi \mathrm{d}\eta}, \Theta_\mathrm{b} = \frac{\int\int \Theta u J \mathrm{d}\xi \mathrm{d}\eta}{\int\int u J \mathrm{d}\xi \mathrm{d}\eta}. \tag{13}$$

The average temperature gradient at the wall is defined as

$$\left.\overline{\frac{\partial \Theta}{\partial \tilde{n}}}\right|_\mathrm{wall} = \frac{\int_{\Gamma_1} \frac{\partial \Theta}{\partial \tilde{n}^{(\xi)}} \sqrt{\alpha_1}\mathrm{d}\eta + \int_{\Gamma_2} \frac{\partial \Theta}{\partial \tilde{n}^{(\eta)}} \sqrt{\gamma_1}\mathrm{d}\xi + \int_{\Gamma_3} \frac{\partial \Theta}{\partial \tilde{n}^{(\xi)}} \sqrt{\alpha_1}\mathrm{d}\eta + \int_{\Gamma_4} \frac{\partial \Theta}{\partial \tilde{n}^{(\eta)}} \sqrt{\gamma_1}\mathrm{d}\xi}{\int_{\Gamma_1} \sqrt{\alpha_1}\mathrm{d}\eta + \int_{\Gamma_2} \sqrt{\gamma_1}\mathrm{d}\xi + \int_{\Gamma_3} \sqrt{\alpha_1}\mathrm{d}\eta + \int_{\Gamma_4} \sqrt{\gamma_1}\mathrm{d}\xi}. \tag{14}$$

The local Fanning friction coefficient C_f=f_F Re is obtained from

$$C_\mathrm{F} = -\frac{D_\mathrm{h}^2 \partial P / \partial \tilde{z}}{2L\mu\bar{u}}. \tag{15}$$

For the uniform wall heat flux boundary conditions, Nu_q is determined by

$$Nu_\mathrm{q} = \frac{1}{\Theta_\mathrm{wall} - \Theta_\mathrm{b}}. \tag{16}$$

2.5. Numerical procedures

The finite-difference scheme is adopted to discrete the governing equation on the computational plane. A line-by-line method is used to solve the resulting algebraic equations. Alternating sweeps of

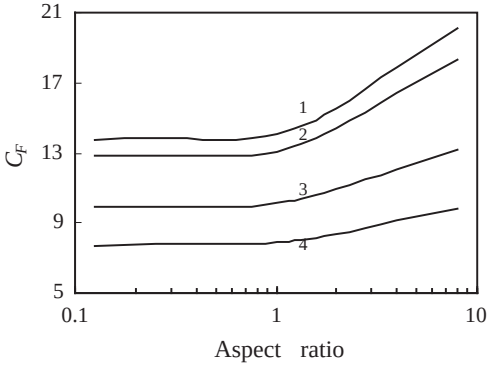

Fig. 2. Variation of the fully developed Fanning friction coefficient C_F with aspect ratio for different $\beta_\nu Kn$. $\beta_\nu Kn$: (1) 0.001, (2) 0.01, (3) 0.05, (4) 0.1; Base angle: 60°.

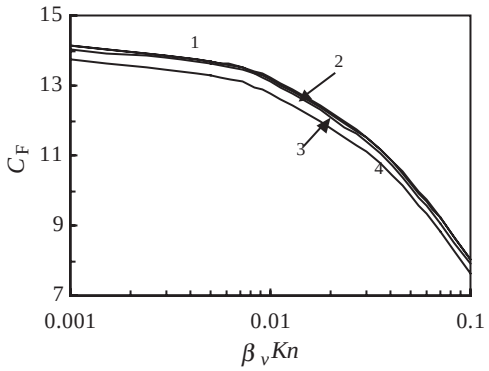

Fig. 3. Variation of the fully developed Fanning friction coefficient C_F with $\beta_v Kn$ for different base angle. Base angle: (1) 90°, (2) 75°, (3) 60°, (4) 45°; Aspect ratio: 1.

tridiagonal matrix algorithm combined with a block correction is applied to each variable. Successive over-relaxation is also employed to improve convergence time.

3. Results and discussion

3.1. Friction coefficient

The effect of rarefaction on the friction coefficient C_F for different aspect ratios and base angles are shown in Figs. 2 and 3. As seen in these figures, C_F decreases with $\beta_v Kn$ for fixed aspect ratio and base angle. Fig. 2 shows that $\beta_v Kn$ has more significant effects on friction coefficient for channel with large aspect ratio. C_F increases with increasing value of aspect ratio when the aspect ratio is larger than 1, while it keeps constant when the aspect ratio is below 1. At high $\beta_v Kn$, the influences of aspect ratio and base angle on friction coefficient become insignificant. Especially, when the aspect ratio is settled, the difference in C_F is very small for base angle bigger than 60°, see Fig. 3.

Fig. 4 shows the friction coefficient as a function of base angle for various aspect ratios. As seen in this figure, C_F increases with increasing of base angles. For ducts with aspect ratio larger than 1, a small base angle has more

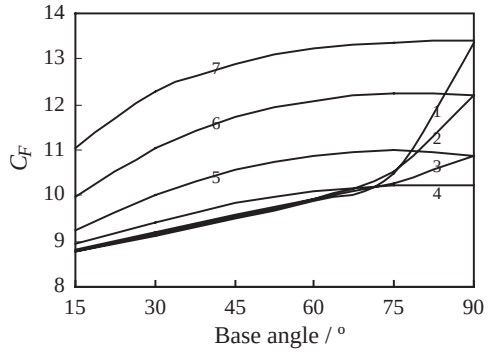

Fig. 4. Variation of the fully developed Fanning friction coefficient C_F with base angle for different aspect ratio. Aspect ratio: (1) 0.125, (2) 0.25, (3) 0.5, (4) 1.0, (5) 2.0, (6) 4.0, (7) 8.0; $\beta_v Kn$: 0.05.

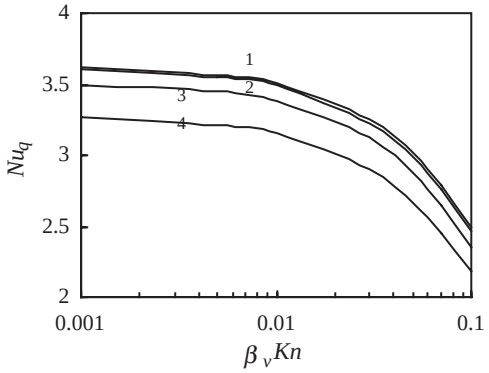

Fig. 5. Variation of the fully developed Nusselt number Nu_q with $\beta_v Kn$ for different base angle. Base angle: (1) 90°, (2) 75°, (3) 60°, (4) 45°; β: 1.667; Aspect ratio: 1.

significant affects on friction coefficient, the influence of base angle on C_F becomes more and more insignificant with the increase of base angle, when base angle is large than 60°, the influence of base angle on C_F can almost be neglected, and C_F approaches asymptotically the value of that of the rectangular channel with same aspect ratio as the base angle increases. When the aspect ratio is below 1, there is little effect of the aspect ratio on friction coefficient for small base angle less than 60°, while for ducts with base angles larger than 60° the friction coefficient changes more sharply with base angle and aspect ratio, C_F quickly approaches the value of rectangular with same aspect ratio as the base angle increases.

3.2. Nusselt number

Figs. 5 and 6 show the effect of rarefaction and cross-section shapes on the developed Nusselt number when $\beta = 1.667$. It is worthwhile pointing out that Nu_q and C_F has similar trends for the same condition shown in Figs. 2–6.

Following to Larrode's [7] and Yu's [8] previous works on slip flow in circular tubes and in rectangular microchannels, we investigate the effect of rarefaction on the heat transfer in trapezoidal microchannel for

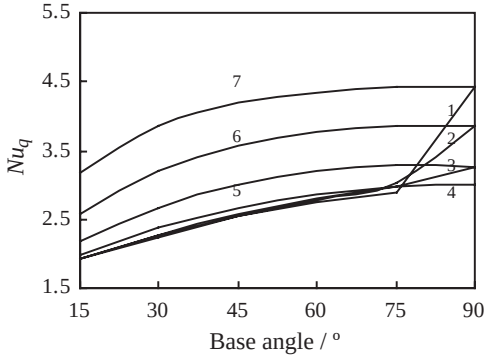

Fig. 6. Fully developed Nusselt number Nu_q *vs*. base angle at different aspect ratio. Aspect ratio: (1) 0.125; (2) 0.25; (3) 0.5; (4) 1.0; (5) 2.0;(6) 4.0; (7) 8.0; $\beta_v Kn$: 0.05, β: 1.667.

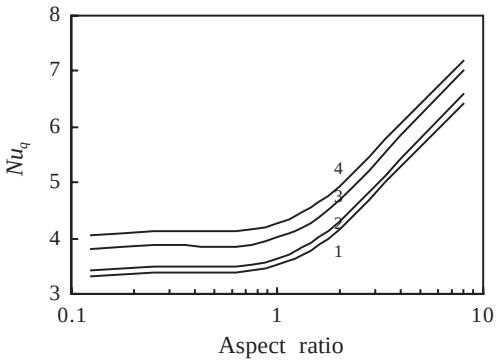

Fig. 7. Fully developed Nusselt number Nu_q vs. aspect ratio at different $\beta_v Kn$. $\beta_v Kn$: (1) 0.001, (2) 0.01, (3) 0.05, (4) 0.1; β: 0.1; base angle: 60°.

three case: $\beta=0.1$, $\beta=0.5$ and $\beta=1.667$. Fig. 7 shows the developed Nusselt number as function of aspect ratios for various base angles at $\beta=0.1$. It is found that Nu_q increases with increasing $\beta_v Kn$ for fixed aspect ratio, but rarefaction has less effect on Nu_q for channels with large aspect ratios. Similar to the trend shown in Fig. 2, Nu_q increase with aspect ratio for aspect ratios larger than 1, and remains constant for aspect ratios below 1. For $\beta=0.5$ (see Fig 8), when the aspect ratio smaller than 1, the effect of $\beta_v Kn$ on Nusselt number is unobvious, while it become significant when the aspect ratio is higher than 1. When $\beta=1.667$, the results in Fig. 9 indicates a different trend from Fig. 7. These performances may be explained by considering the physical characteristics of velocity slip and temperature jump. Velocity slip increases the fluid velocity at the wall, enhancing convection heat transfer between the fluid and the wall; while temperature jump decreases temperature gradients at the wall, reducing the heat transfer between the fluid and the wall. When the value of β is small, temperature jump is negligible compared with velocity slip, the heat transfer is controlled only by velocity slip, and so it is enhanced. For high β, the temperature jump is very significant, and it suppresses the enhancement of heat transfer due to velocity slip, so the Nusselt number decreases.

The results presented in Figs. 10 and 11 show the influence of β on heat transfer as a function of aspect ratio and base angles. It is evident that convection heat transfer decreases with increasing the value of β. When β is small, velocity slip enhances the heat transfer between the fluid and the wall; the developed Nusselt number is

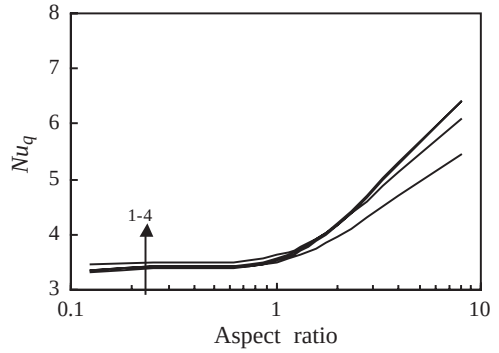

Fig. 8. Fully developed Nusselt number Nu_q *vs*. aspect ratio at different $\beta_v Kn$. $\beta_v Kn$: (1) 0.001, (2) 0.01, (3) 0.05, (4) 0.1; β: 0.5; base angle: 60.

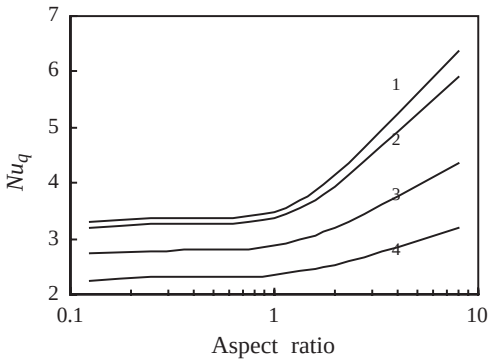

Fig. 9. Fully developed Nusselt number Nu_q vs. aspect ratio at different $\beta_v Kn$. $\beta_v Kn$: (1) 0.001, (2) 0.01, (3) 0.05, (4) 0.1; β: 1.667; base angle: 60°.

larger than the value of no-slip flow. While for large β, heat transfer is suppressed by the temperature jump at the wall; thus, Nusselt number is smaller than $Nu_{\text{no-slip}}$. Specifically, as β increases, the Nu_q profile in Figs. 10 and 11 become more and more flat. The result reveals that the effects of aspect ratio and base angle on heat transfer are less obvious at large temperature jump.

4. Conclusions

Fully developed laminar flow and heat transfer for trapezoidal microchannel over the entire slip flow regime has been studied. Uniform wall heat flux boundary conditions were considered in this simulation. The friction coefficient in slip flow region was reduced in comparison with the no-slip flow results. The effects of aspect ratio and base angle on friction coefficient become less obvious at high $\beta_v Kn$. For small β, convection heat transfer is controlled by velocity slip at the wall, the developed Nusselt number is larger than the value of no-slip flow. While for large β, temperature jump dominates the heat transfer between the fluid and the wall, Nusselt number is smaller than

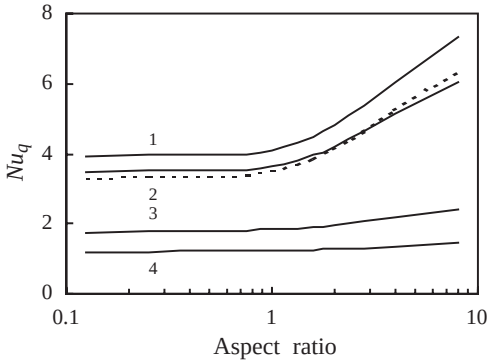

Fig. 10. Fully developed Nusselt number Nu_q vs. aspect ratio at different β. β: (1) 0, (2) 0.5, (3) 5, (4) 10; $\beta_v Kn$: 0.05; base angle: 60°; - - -, no-slip flow.

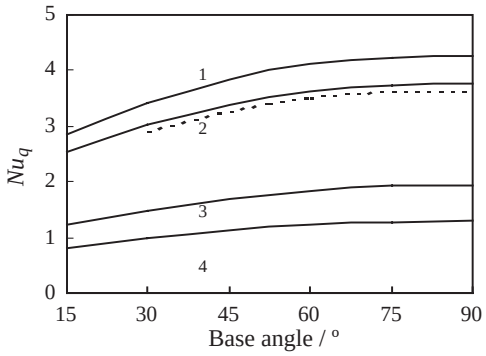

Fig. 11. Fully developed Nusselt number Nu_q vs. base angle at different β. β: (1) 0, (2) 0.5, (3) 5, (4) 10; $\beta_v Kn$: 0.05; Aspect ratio: 1; - - -, no-slip flow.

$Nu_{\text{no-slip}}$. The influences of aspect ratio and base angle on heat transfer are insignificant for large temperature jump.

Nomenclature

D_h	hydraulic diameter (m)
L	length of duct (m)
P	pressure (Pa)
k	thermal conductivity of fluid (W m^{-1} K^{-1})
q	heat generation per unit area (W m^{-2})
u	axial velocity (m s^{-1})
$\bar{u}$	average velocity
β_v	dimensionless variable defined in Eq. (6)
β_T	dimensionless variable defined in Eq. (6)
β	dimensionless variable $\beta=\beta_T/\beta_v$
γ	specific heat ratio
μ	viscosity (Pa s)
Θ	dimensionless temperature Eq. (4)
σ_v	tangential momentum accommodation coefficient
σ_T	thermal accommodation coefficient
ε	ratio of channel hydraulic diameter to its length
Γ	boundaries of computational domain
θ	base angle (degree)

Acknowledgements

We gratefully acknowledge the financial support of the National Natural Science Foundation of China (Nos. 20176057, 20122201 and 20490200), the Key Program for International Cooperation of Science

and Technology (No. 2001CB711203) and the Knowledge Innovation Program of the Chinese Academy of Sciences (No. K2003E2).

References

[1] K.F. Jensen, AIChE J. 45 (10) (1999) 2051.
[2] P. Wu, W.A. Little, Cryogenics (1984) 415.
[3] J. Harley, J. Pfahler, H. Bau, J.N. Zemel, Transport processes in micron and sub-micron channels, Proc. ASME Heat Transp. Process. HTD 116 (1989) 1.
[4] J. Pfahler, J. Harley, H. Bau, J.N. Zemel, Proc. ASME Micromech. Sens., Actuators, Syst. DSC 31 (1991) 49.
[5] S.B. Choi, R.F. Barron, R.O. Warrington, Proc. ASME DSC 32 (1991) 123.
[6] E.B. Arkilic, M.A. Schmidt, J. Microelectromechanical Syst. 6 (2) (1997) 167.
[7] F.E. Larrode, C. Housiadas, Y. Drossinos, Int. J. Heat Mass Transfer 43 (2000) 2669.
[8] S.P. Yu, T.A. Ameel, Int. J. Heat Mass Transfer 44 (2001) 4225.
[9] H.Y. Wu, P. Cheng, Int. J. Heat Mass Transfer 46 (2003) 2519.
[10] W.Q. Tao, Numerical Heat Transfer, Second edition, The Xian Jiao Tong University Press, Xi An, 2001.